Mem. S.A.It. Vol. 85, 371

Memorie della

The exchange of metals between galaxies and the intergalactic medium at high redshift

E. Scannapieco

School of Earth and Space Exploration, Arizona State University, PO Box 876004, Tempe - 85287, USA, e-mail: evan.scannapieco@asu.edu

Abstract. I discus several important issues in the exchange of metals between galaxies and the intergalactic medium at high redshift. The ejection of metals from galaxies appears to be more efficient at high-redshift than today, as can be understood not only because of the smaller gravitational potential wells of galaxies, but also because of their more compact sizes, spatial distribution, and the overall expansion of the universe. By $z \approx 2$, intergalactic enrichment at appears to be concentrated around large galaxies and this is likely due primarily due to metals from similarly-biased higher-redhishift sources, although ongoing studies using pairs of quasar sight lines are necessary to settle this issue definitively. Finally, I discuss the mixing of metals, which occurs through a turbulent cascade similar to the Kolmogorov energy cascade. Our direct simulations of this process have yielded sub-grid models that can track the formation history of metal-free stars.

Key words. Galaxy: abundances – IGM: abundances – Stars: Population III

1. Introduction

Big bang nucleosynthesis produced helium efciently, as well as trace amounts of the light elements lithium, beryllium, and boron (e.g. Walker et al. 1991). On the other hand, heavier elements, the metals, were produced by stars, which formed within the densest regions of galaxies. This would seem to imply that metals would be heavily concentrated to the most dense regions of the Universe, but in fact this is not the case. Instead, metal pollution is ubiquitous. Even the most pristine stars Milky Way halo stars have been polluted by previous stellar generations (e.g. Cayrel et al. 2004; Frebel et al. 2008; Caffau et al. 2011), and even the most tenuous of regions of the intergalactic medium (IGM), while not uniformly enriched, are often found to contain metals (e.g. Schaye et al. 2003; Pieri et al. 2010).

How and when this intergalactic material was first enriched is a question that directly impacts our understanding of many issues, including galaxy feedback, as the enriched IGM retains a fossil record of the material ejected from galaxies, gas accretion onto galaxies, as cooling is strongly-dependent on metallicity (e.g. Sutherland & Dopita 1993), and the history of star formation, as stars that formed from metal-free gas are likely to have properties that were extremely different from the stars in the present-day Universe (e.g. Bromm & Larson 2004). In this contribution, I will discuss the high-redshift stage of this process, focusing on three major issues: the ejection and propagation of metals at high-redshifts, how this processes can be constrained by the clustering measurements of quasar absorption lines, and the mixing and homogenization of enriched material by turbulence.

2. The ejection and propagation of metals at high-redshift

From $z = 0$ to 2.5, the gas-phase metallicity of galaxies is observed to depend on stellar mass, M^* and star formation rate (SFR) as $Z \propto M^*(SFR)^{-1/3}$, implying that galaxies are much less efficient at enriching their interstellar media if they have low masses or are rapidly forming stars (Mannucci et al. 2010) (see also Tremonti et al. 2004). The dependence on M^* can be understood as occurring because gas heated by supernovae and stellar winds has an easier time escaping smaller gravitational potential wells. The dependence on SFR, on the other hand, can be explained either by dilution due to infall of low-metallicity gas onto the galaxies that are rapidly forming stars, or by increased efficiency of metal ejection from galaxies with high star-formation rates.

Indeed, large outflows are ubiquitous in galaxies in which the global star-formation rate density per unit area exceeds a critical value of $\dot{\Sigma}_* \approx 0.1$ M$_\odot$ yr^{-1} kpc^{-2} (Heckman 2002). Interestingly, the X-ray properties of such outflowing galaxies are similar over a very large mass range (Grimes et al. 2005), suggesting that a common physical mechanism is producing this emission in all starbursts. The critical star formation rate density, which corresponds to a gas surface density of ≈ 50 M$_\odot$ pc^{-2}, can also be understood as arising from the Toomre stability criterion (Toomre 1964), which relates the disk surface density, epicyclic frequency, and vertical pressure support. Because a significant fraction of the vertical support arises from turbulence (e.g. Elmegreen & Scalo 2004), high $\dot{\Sigma}_*$ galaxies also correspond to strongly turbulent disks (e.g. Genzel et al. 2011). Furthermore, as shown in Figure 1, once turbulence becomes vigorous enough, exceeding a critical 1D velocity dispersion ≈ 35 km/s, a runaway process develops.

This occurs because turbulent dissipation does not heat the gas uniformly, but rather deposits only a small amount of energy in some regions, while heating other regions to several times the mean temperature. As the efficiency of cooling drops sharply above $\approx 2\times10^5$ K, the portion of the gas that is heated to above this value takes several turbulent dissipation timescales to cool. This means that before the overheated gas can settle back down to the mean temperature, subsequent turbulent energy input will heat it even further, causing it to expand to maintain pressure equilibrium with its surroundings. Both the increased temperature and lower density lead to even less efficient cooling, and this causes the rapid, runaway heating of the hot, low-density gas, which pushes its way out of the galaxy, dragging a substantial portion of the total gas mass with it. In other words, it is impossible to balance turbulent dissipation by radiative cooling in highly-turbulent, rapidly star-forming galaxies (Scannapieco et al. 2012), and the result is that the highest $\dot{\Sigma}_*$ galaxies naturally eject a large fraction of the high-metallicity material generated by massive stars (Scannapieco 2013).

Extrapolating this process to higher redshifts, when galaxies were much more compact than today (e.g. Oesch et al. 2010), implies that early galaxies were much more efficient at ejecting metals. In fact, above $z = 2.5$ metallicities begin to drop even below the levels expected due to their smaller masses and high star formation rates, such that galaxies systematically fall 0.6 dex below the lower redshift $Z \propto M^*(SFR)^{-1/3}$ relation. Furthermore, beyond the ease in ejecting material from the galaxies themselves, several cosmological effects also help to aid in the propagation of metals at high redshift (Scannapieco 2005; Porciani & Madau 2005).

To see why this is the case, consider an extremely simple model of a galaxy outflow as a Sedov-Taylor blast wave with an energy E, such that its radius R will evolve as $R \propto (E/\rho)^{1/5}\, t^{2/5}$, where ρ is the density of the surrounding medium and t is the time since the blast wave has gone off. Since $\rho \propto (1 + z)^3$ even ignoring the fact that t will be longer

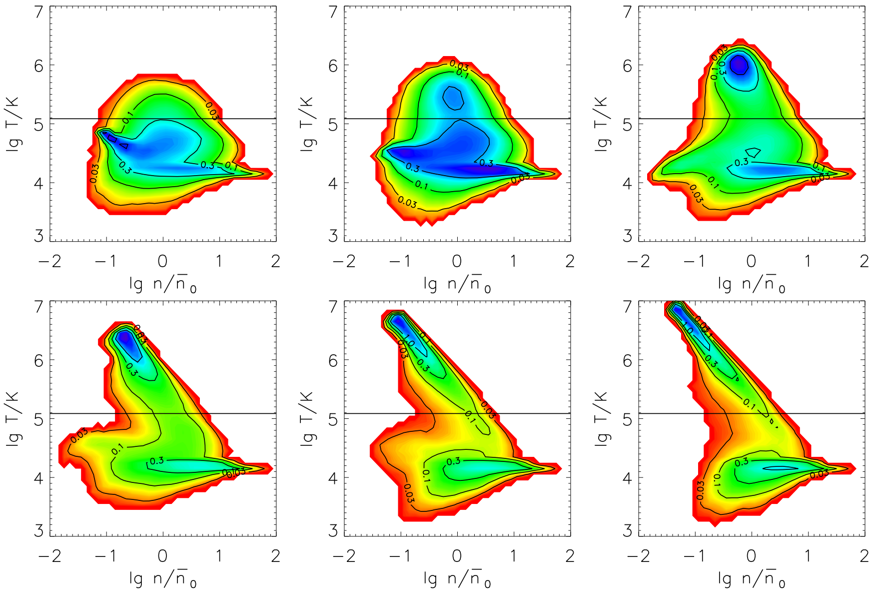

Fig. 1. Phase diagram showing logarithmic contours of the mass-weighted Probablity Distribution Function (PDF) of the gas distribution in a run which approximates the evolution of a portion of a disk galaxy with a 1-D velocity dispersion 34 km/s. All contours are labeled by their values relative to the PDF bin with the most mass. From left to right and top to bottom the panels correspond to evenly-spaced snapshots taken from 1 to 6 eddy turnover times.

for higher-redshifts source, this means that the comoving radius of a blast wave will go as $r_{\rm com} \propto (1+z)^{2/5}E^{1/5}$, or in other words, since the Universe is more compact at high-redshift, it is much easier for a blast-wave of equivalent strength to reach a larger comoving distance.

For similarly biased sources at different redshifts, the number density goes as $1/M$, and this means that the IGM filling factor due to sources with energy M and energy E should go as $(1+z)^{6/5}E^{3/5}/M$. When coupled with the arguments above, which suggest that the fraction of energy released by stars that is channeled into a galaxy outflow is much higher when M is small or z is high, it is clear that it is much easier to enrich large volumes of the intergalactic medium with low mass, early sources, than with larger galaxies in the moderate redshift to present-day Universe.

On the other hand, the overall observed star-formation rate density in the Universe drops slowly with increasing redshift above $z \approx 3$, and rapidly with increasing redshift above $z \approx 7$ (e.g. Oesch et al. 2013), meaning that if one pushes to to high enough redshifts, there are too few stars to generate any significant metalsl. Perhaps the best tool in disentangling this competition between increased efficiency of ejection and propagation of metals at early times, and higher overall metal production rates at later times is the spatial distribution of intergalactic metals.

3. Observations of the intergalactic metal distribution

From absorption-line studies of distant quasars, one can obtain column density measurements of the neutral hydrogen distribution (the Lyman-α Forrest) as well as the distribution of a variety of metal ions, identified as doublets. In another contribution in this volume (Fumagalli 2013), a variety of approaches to studying this data by examining the relation between the hydrogen and metal-line distributions are reviewed. These include the pixel optical depth method (e.g. Cowie & Songaila 1998; Schaye et al. 2003), which relies on directly comparing the optical depths of the hydrogen and metal-line absorbers, analyses of individual Lyα forest lines (e.g. Simcoe 2011), and analyses of composite quasar spectra (e.g. Pieri et al. 2010). Here we discuss an alternative approach, using the clustering properties of IGM metals to contain the sources from which they originated.

Because the galaxies that enriched the IGM formed in dense regions of space, they are more clustered than the overall matter distribution. Furthermore, this biasing is a systematic function of the masses and redshifts of these structures (Kaiser 1984). Thus, information from the large scale clustering of metal absorbers provides valuable insight into the objects from which metals were ejected.

In Scannapieco et al. (2006), we studied this spatial distribution in high-resolution (R= 45000), high signal-to-noise (60-100 pixel^{-1}) *Very Large Telescope* (*UVES*) spectra of absorbers at redshifts $z = 2 - 3$, as traced by the species C IV, Si IV, Mg II, and Fe II. For each of these species we computed a line-of-sight correlation function in redshift space, $\xi_{\rm los}(v)$, defined as the excess probability of finding a pair of metal absorbers at a velocity separation v. The correlation functions all had high amplitudes and a knee at $\approx$ 150 km/s (see also Steidel 1990; Petitjean & Bergeron 1994; Rauch et al. 1996). These features did not depend on absorber column densities and by comparing them with a suite of smoothed particle hydrodynamic simulations, we found that these measurements were consistent with bubbles of metals that were $\approx$ 2 comoving Mpc in radius, surrounding dark matter halos with masses $\approx 10^{12} M_\odot$, similar to Lyman-break galaxies (Adelberger et al. 2005).

However, the clustering of metals is difficult to interpret unambiguously along single lines of sight, because distance and velocity information are mixed in redshift space, such that it is unclear if the $\approx$ 150 km/s knee in $\xi_{\rm los}(v)$ was due to extremely large enriched regions, which would suggest overlapping bubbles from high-redshift sources biased like Lyman break galaxies, or from ongoing winds, which would suggest single bubbles from Lyman-break galaxies themselves. To overcome this degeneracy, we made use of a sample of 29 quasar pairs, with redshifts between 1.7-4.3 and separations from $\approx$ 0.1 to 2 comoving Mpc (Martin et al. 2010), which were selected from the sample in Hennawi et al. (2010). Spectra for each pair were taken with the ESI spectrograph on Keck II, which provided a resolution of 60 km/s. These then allowed us to compare the distribution of metal transverse to the line-of-sight, breaking the degeneracy between velocity and distance.

As shown in the upper left panel of Figure 2, computing the distributions of velocity differences of C IV absorbers along the individual sightlines from this data yielded a line-of-sight correlation function that was consistent with the Scannapieco et al. (2006) *UVES* results. As expected from this line-of-sight clustering, we also found many more pairs of C IV absorbers at similar redshifts in neighboring sightlines than would occur randomly. We quantified this using the projection

$$w(r_P, \Delta v_{\rm pair}) \equiv \int_{-\Delta v_{\rm pair}}^{+\Delta v_{\rm pair}} \xi(r_P, v)\, dv, \qquad (1)$$

where $\xi(r_P, v)$ is the correlation function of absorbers separated by a transverse comoving distance r_p and a velocity difference v, show in the lower left panel of Figure 2. At the largest separations the transverse C IV systems clustered similarly to the line-of-sight correlation function, while at small separations the transverse results again deviated from a power law.

To analyze these results we assumed a real-space correlation function of the form

$$\begin{aligned} \xi(r) &= (r_0/r)^\gamma \text{ for } r \geq r_1 \\ & (r_0/r_1)^\gamma \text{ for } r < r_1, \end{aligned} \qquad (2)$$

and, appropriately accounting for infall, attempted to simultaneously fit r_1 and r_0 to the line-of-sight and transverse data, as shown in the right panels of Figure 2. The transverse data favored large correlation lengths, $r_0 \geq 4$ comoving Mpc h^{-1} and large sizes of enriched regions $r_1 \geq 0.5$ comoving Mpc h^{-1}, where h

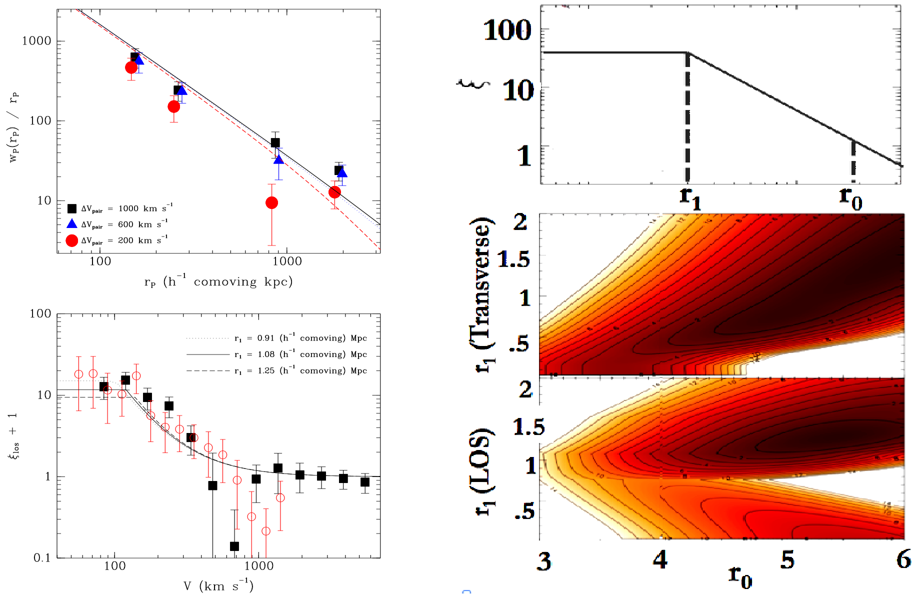

Fig. 2. *Left, Top:* Correlation function of C IV absorption systems vs. line-of-sight distance. The *ESI* data (squares, Martin et al. 2010) agree with the earlier *VLT* data (red circles, Scannapieco et al. 2006). The bins near 500 km s^{-1} have a small number of systems, and fits are for models fixing $r_0 = 4.0\,h^{-1}$ comoving Mpc and $\gamma = 1.6$ with different values of r_1 as defined in Eqn. 2 and illustrated in the Right, Top panel. *Left, Bottom:* Transverse C IV correlation function normalized by sightline separation versus median sightline separation. The lines show the projection of the galaxy-galaxy correlation function at $z \simeq 2.9$ (Adelberger et al. 2005), extrapolated below 1 h^{-1} comoving Mpc with a constant power-law index $\gamma = 1.6$, perturbed by linear infall. *Right, Top:* Illustration of the two-parameter real-space correlation function fit to the data. The correlation length r_0 and the size of enriched regions r_1 parameterize Eqn. 2, and the power-law index, $\gamma = 1.6$, is taken to be fixed. *Right, Bottom:* Contours of $\Delta\chi^2$ for two-parameter fits to the C IV correlation function. The fitted transverse and line-of-sight C IV correlation functions are illustrated separately in the upper and lower panels, respectively. The contours indicate values of $\Delta\chi^2$, where 2.3, 4.6, and 6.2 correspond to the 68%, 90%, and 95% confidence levels. Adopting the $r_0 \approx 4\,h^{-1}$ comoving Mpc clustering length of Lyman-break galaxies implies the presence of ≈ 100 km s^{-1} peculiar velocities amongst C IV systems. Larger values of the correlation length require smaller velocities. No Doppler shifts are required if the correlation length exceeds 6 h^{-1} comoving Mpc and $r_1 \simeq 1.3\,h^{-1}$ comoving Mpc (From Martin et al. 2010).

is the Hubble constant in units of 100 km s^{-1} Mpc $^{-1}$. This places limits on the level to which peculiar velocities caused by ongoing outflows can effect the data.

If one adopts a small value of $r_0 \approx 4$, comoving Mpc h^{-1}, consistant with the clustering length of Lyman-break galaxies, then this implies small peculiar velocities among C IV systems on the order of ≈ 100 km/s. Larger values of the correlation length, which are somewhat favored if one allows for r_0 to be be fit freely, require no ongoing outflows to fit the full data set. Even more importantly, the data can not be fit at all if one allows for average outflows speed larger than ≈ 300 km s^{-1}. From this limit on the outflow speed and the minimum size of enriched regions, the timescale for dispersing metals exceeds a Gyr. This is much longer than the typical stellar ages of Lyman-break galaxies and suggests that $z \geq 4.5$ sources played a central role in dispersing metals. These constraints can be improved by increasing the sample with other pairs, which have already been observed and will be analyzed by our group in the near future.

4. Metal mixing

Finally, we consider the mixing of enriched material into a lower-metallicy environment. Understanding this process is essential not only for understanding the incorporation of metals into the IGM, but also for interpreting a wide range of observations including the cluster to cluster metallicity scatter (e.g. Twarog et al. 1997) and the scatter in metallicities and abundance ratios in coeval field stars (e.g. Nordström et al. 2004). In each of these systems, the degree of chemical inhomogeneity is controlled by the efficiency with which metals are transported and mixed by turbulence (Scalo & Elmegreen 2004).

While turbulent mixing in incompressible fluids has been extensively studied in the fluid dynamics literature, where it is usually referred to as passive scalar turbulence (e.g. Shraiman & Siggia 2000), there have been very few studies in the supersonic regime essential to astrophysics. The incompressible picture, known as the Obukohov-Corrsin phenomenology, is a cascade of scalar fluctuations caused by the stretching of the concentration field by the velocity field. This produces structures of progressively smaller size, down to the scale at which molecular diffusion homogenizes and erases the fluctuations in abundances. In fact, molecular diffusion is the only process responsible for true mixing, but it operates very slowly at the large scales at which scalar sources are injected. By providing a path from the scalar injection scale to the diffusion scale, the cascade process greatly accelerates mixing.

In Pan & Scannapieco (2010, 2011) we carried out the first systematic numerical study of passive scalar mixing in isothermal supersonic turbulence, yielding several important results. To study this process we ran a suite of 512^3 simulations of isothermal, homogenous turbulence in a periodic box, using the FLASH code (Fryxell et al. 2000). The flow velocity was continuously driven on large scales by a stochastic forcing term, whose amplitude was adjusted to achieve different Mach numbers, and metals were similarly added stochastically on large scales throughout the simulation.

Our results showed that the ratio of the scalar mixing timescale, τ_c, to the flow dynamical time, τ_{dyn}, (defined as the flow driving scale divided by the rms velocity), increases with the Mach number, M, for $M \leq 3$, and then becomes almost constant for higher Mach numbers. This trend suggests that compressible modes of turbulence are less efficient in enhancing mixing than solenoidal modes. However, at all Mach numbers, τ_c is close to τ_{dyn} and the overall change in τ_c/τ_{dyn} is less than 20% over the range $1 \leq M \leq 6$, which suggests that scalar mixing is driven by a cascade process similar to that of the velocity field, regardless of Mach number.

Furthermore, the extension of the scalar cascade picture to the supersonic regime predicts a relation between the scaling exponents of the velocity and the scalar structure functions, which characterize the degree of turbulent structures as a function of scale. In particular, the scalar structure function becomes flatter with Mach number, indicating more small-scale metal fluctuations, and the velocity scaling steepens, indicating less small-scale velocity fluctuations. This is because at higher Mach numbers, the presence of shocks causes large-scale motions to be dissipated directly to thermal energy, causing a deficit of smaller scale motions, which slows mixing on smaller scales.

Building on this study, in Pan et al. (2013), we carried out studies of the mixing of metals into primordial gas, to track the unresolved fraction of "pristine" gas in every cell in a high-redshift cosmological simulation. As discussed above, stars forming from metal-free gas are thought to have had very different properties than later stellar generations, which formed only after the first stars polluted the surrounding turbulent interstellar gas beyond a critical metallicity, Z_c, between 10^{-6} and 10^{-3} $Z_\odot$. This critical value is much smaller than the typical overall average metallicity, and therefore the mixing efficiency of the pristine gas in the interstellar medium plays a crucial role in determining the transition from Pop III to normal star formation.

With the goal of developing a subgrid model for tracking the evolution of the first

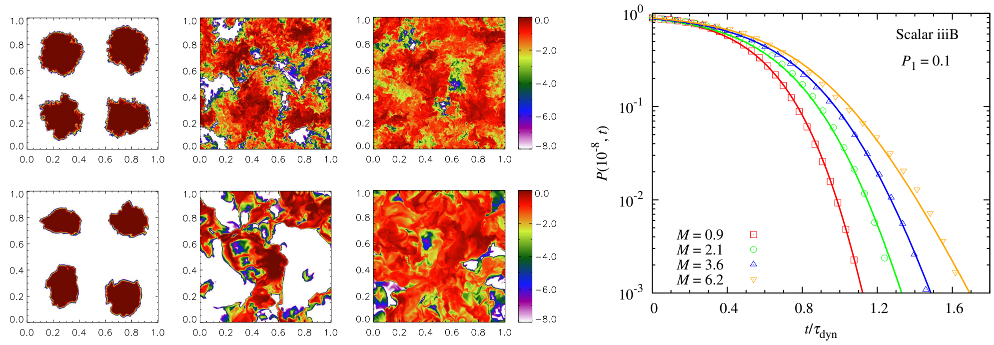

Fig. 3. *Left:* metal concentration with mass fraction below 10^{-8}. From left to right, the top three panels show snapshots of the simulation volume in Mach 0.9 flow at t = 0.1, 0.7 and 1.1 dynamical times. The initial condition of this scalar field is eight equally-spaced blobs with a total pollutant fraction of 10%. The lower three panels plot the metallicity field with the same initial condition but in highly supersonic, Mach 6.2 turbulence. *Right:* The pristine fraction as a function of time for eight equally-spaced blobs with a total pollutant fraction of 10%, for four simulated flows at Mach 0.9, 2.1, 3.5 and 6.2. Lines are fitting functions based on the predictions of self-convolution models (From Pan et al. 2013).

stars, we carried out a detailed numerical and theoretical investigation of the fundamental physics of the pollution of pristine fluid elements in isotropic compressible turbulence, such as occurs in and around the highest-redshift galaxies. This again involved simulating isothermal turbulence in a 512^3 box, but in this case, as illustrated in the left panels of Figure 3, we focused on the evolution of the fraction of gas below Z_c as a function of time. While the evolution of the metallicity distribution function in a turbulent medium cannot be solved exactly, in Pan et al. (2012) we derived predictions for the evolution of the metal-free fraction for several closure models from the literature, and showed that a class of models, called self-convolution models (Venaille & Sommeria 2007; Duplat & Villermaux 2008), provided successful fitting functions that matched our numerical results (see Fig. 3, right panel).

These models are based on the physical picture of turbulent stretching causing a cascade of metallicity structures toward the small scales at which molecular diffusivity can efficiently operate as a convolution between polluted and unpolluted material. The models are dependent only on two major parameters: $\tau_{\rm con}$, which sets the characteristic timescale for the convolution of the metal abundance PDF through turbulent stretching of concentration structures, and n, which quantifies the degree of spatial locality of the PDF convolution process. Using a suite of numerical simulations to expand these results, we were not only able measure $\tau_{\rm con}$, and n for all pollutant conditions relevant for primordial star formation, but also derive an extremely simple equation for the evolution of the pristine fraction throughout the simulations:

$$\frac{D(\rho P)}{Dt} = \frac{\partial}{\partial x_i}\rho\gamma_{\rm P}\frac{\partial P}{\partial x_i} - \frac{nP\left(1-P^{1/n}\right)}{\tau_{\rm scon}} - \dot{m}_{\rm ej}P, \quad (3)$$

where, ρ is the density of the gas, P is the primordial fraction, v is the velocity field, $\dot{m}_{\rm ej}$ is the rate at which SN ejecta are being released, $\gamma_{\rm P}$ is the turbulent diffusion rate, which is proportional to the velocity times the length scale of the turbulence, and we have fit n and $\tau_{\rm scon}$ with simple functions of the local turbulent Mach number and average metallicity. This makes it just as easy to track the fraction of primordial gas in each zone in a simulation,as it is to track its average metallicity. With this tool, we are currently carrying out cosmological simulations that can track the formation of metal free stars even in regions in which the mean metallicity is high, but material is not yet mixed, helping to shed further light on one of the many outstanding questions in the history of metals enrichment at high redshift.

Acknowledgements. I would like to thank the organizers of this interesting and enjoyable conference, and also thank my collaborators on the work described here: B. Aracil, J. Bergeron, H. Couchman, S. G. Djorgovski, S. Ellison, A. P. Fournier, W. J. Gray, J. Hennawi, L. Pan, P. Petitjean, C. Pichon, D. Pogosyan, C. Martin, J. Scalo, & R. J. Thacker. I acknowledge support from NASA under theory Grant No. NNX09AD106 and the National Science Foundation under grant AST 11-03608.

References

Adelberger, K. L., Shapley, A. E., Steidel, C. C., et al. 2005, ApJ, 629, 636
Bromm, V., & Larson, R. B. 2004, ARA&A, 42, 79
Caffau, E., Bonifacio, P., François, P., et al. 2011, Nature, 477, 67
Cayrel, R., Depagne, E., Spite, M., et al. 2004, A&A, 416, 111
Cowie, L. L., & Songaila, A. 1998, Nature, 394, 44
Duplat, J., & Villermaux, E. 2008, Journal of Fluid Mechanics, 617, 51
Elmegreen, B. G., & Scalo, J. 2004, ARA&A, 42, 211
Frebel, A., et al. 2008, ApJ, 684, 588
Fryxell, B., Olson, K., Ricker, P., et al. 2000, ApJS, 131, 273
Fumagalli, M. 2013, arXiv:1312.5321
Genzel, R., Newman, S., Jones, T., et al. 2011, ApJ, 733, 101
Grimes, J. P., et al. 2005, ApJ, 628, 187
Heckman, T. M. 2002, Extragalactic Gas at Low Redshift, 254, 292
Hennawi, J. F., Myers, A. D., Shen, Y., et al. 2010, ApJ, 719, 1672
Kaiser, N. 1984, ApJ, 284, L9
Kennicutt, R. C., Jr. 1998, ARA&A, 36, 189
Mannucci, F., et al. 2010, MNRAS, 408, 2115
Martin, C. L., Scannapieco, E., Ellison, S. L., et al. 2010, ApJ, 721, 174
Nordström, B., Mayor, M., Andersen, J., et al. 2004, A&A, 418, 989
Oesch, P. A., Bouwens, R. J., Carollo, C. M., et al. 2010, ApJ, 709, L21
Oesch, P. A., Bouwens, R. J., Illingworth, G. D., et al. 2013, ApJ, 773, 75
Pan, L., & Scannapieco, E. 2010, ApJ, 721, 1765
Pan, L., & Scannapieco, E. 2011, Phys. Rev. E, 83, 045302
Pan, L., Scannapieco, E., & Scalo, J. 2012, J. of Fluid Mech., 700, 459
Pan, L., Scannapieco, E., & Scalo, J. 2013, ApJ, 775, 111
Petitjean, P., & Bergeron, J. 1994, A&A, 283, 759
Pieri, M. M., Frank, S., Mathur, S., et al. 2010, ApJ, 716, 1084
Scalo, J., & Elmegreen, B. G. 2004, ARA&A, 42, 275
Schaye, J., Aguirre, A., Kim, T.-S., et al. 2003, ApJ, 596, 768
Shraiman, B. I., & Siggia, E. D. 2000, Nature, 405, 639
Simcoe, R. A. 2011, ApJ, 738, 159
Porciani, C., & Madau, P. 2005, ApJ, 625, L43
Rauch, M., et al. 1996, ApJ, 467, L5
Scannapieco, E. 2005, ApJ, 624, L1
Scannapieco, E. 2013, ApJ, 763, L31
Scannapieco, E., Pichon, C., Aracil, B., et al. 2006, MNRAS, 365, 615
Scannapieco, E., Gray, W. J., & Pan, L. 2012, ApJ, 746, 57
Schaye, J., Aguirre, A., Kim, T.-S., et al. 2003, ApJ, 596, 768
Steidel, C. C. 1990, ApJS, 72, 1
Sutherland, R. S., & Dopita, M. A. 1993, ApJS, 88, 253
Toomre, A. 1964, ApJ, 139, 1217
Tremonti, C. A., Heckman, T. M., Kauffmann, G., et al. 2004, ApJ, 613, 898
Twarog, B. A., Ashman, K. M., & Anthony-Twarog, B. J. 1997, AJ, 114, 2556
Venaille, A., & Sommeria, J. 2007, Physics of Fluids, 19, 028101
Walker, T. P., et al. 1991, ApJ, 376, 51